

Quantum-correlated photons generated by nonlocal electron transport

Felicitas Hellbach,¹ Fabian Pauly,² Wolfgang Belzig,¹ and Gianluca Rastelli^{1,3}

¹*Fachbereich Physik, Universität Konstanz, 78457 Konstanz, Germany*

²*Institute of Physics, University of Augsburg, 86135 Augsburg, Germany*

³*INO-CNR BEC Center and Dipartimento di Fisica, Università di Trento, 38123 Povo, Italy*
(Dated: October 26, 2021)

Since the realization of high-quality microwave cavities coupled to quantum dots, one can envisage the possibility to investigate the coherent interaction of light and matter in semiconductor quantum devices. Here we study a parallel double quantum dot device operating as single-electron splitter interferometer, with each dot coupled to a local photon cavity. We explore how quantum correlation and entanglement between the two separated cavities are generated by the coherent transport of a single electron passing simultaneously through the two different dots. We calculate the covariance of the cavity occupations by use of a diagrammatic perturbative expansion based on Keldysh Green's functions to the fourth order in the dot-cavity interaction strength, taking into account vertex diagrams. In this way, we demonstrate the creation of entanglement by showing that the classical Cauchy-Schwarz inequality is violated if the energy levels of the two dots are almost degenerate. For large level detunings or a single dot coupled to two cavities, we show that the inequality is not violated.

I. INTRODUCTION

Nonlocality is a fundamental property of quantum mechanics that manifests itself in two main ways: as delocalization of a quantum particle in space according to its associated wave function (superposition), as correlations between spatially separated parts of a quantum system (entanglement). It is at the heart of quantum communication and computing in various physical implementations.

An intriguing example of quantum delocalization is the interference in the motion of a single electron. Quantum delocalized transport has been proven in nanodevices formed by two possible paths connecting an initial and final point, namely two electrical contacts playing the role of source and drain. Examples are parallel double dots [1–3], operating as single-electron splitter interferometer, or the electronic Mach-Zehnder interferometer, operating with the edge states of two-dimensional (2D) quantum Hall systems [4]. Similarly to a photon in a Mach-Zehnder interferometer, an electron wave-function can split in two branches and then by recombining give rise to interference in the transmitted flux. In general, semiconducting single-electron devices form a unique playground to address nonlocal electron transport and quantum interference [1–3, 5, 6].

Beside electron transport, quantum mechanics can be explored at high precision in the field of optics, and microwave quantum photonics has made remarkable progress in the last decade. In the circuit quantum electrodynamics (QED) architecture [7], arbitrary quantum states in an electromagnetic microwave resonator can be prepared and measured [8, 9]. Moreover, using superconducting qubits or Josephson circuitry (Josephson parametric amplifier or wave-mixer), quantum entangled states of microwave photons have been realized in two spatially separated resonator cavities [10], in two resonator modes of different frequency [11, 12] as well as

in propagating photons [13–15]. More recently, an entangled pair of two-mode cat states has been realized in two microwave cavities [16], and a dc-biased Josephson junction created two continuous entangled microwave beams [17].

Beyond superconducting circuits based on Josephson junctions, quantum dots realized in semiconducting nanostructures implement reliable and well-controlled qubits [18, 19] with transition frequencies in the microwave domain and with the advantage of electric field control [20]. Quantum dots can now be readily coupled to microwave photon cavities, establishing the field of semiconductor hybrid QED [21], which provides a novel family of coherent quantum devices that combine electronic with photonic degrees of freedom on-chip [22–32]. The so-called strong coupling regime has been reached [33–35] as well as the full microwave control and readout of the quantum dot qubits [36].

Coupling quantum dots with quantum optical resonators adds a new dimension to the cavity and circuit QED, beyond the conventional paradigm of an atom coupled to a harmonic oscillator. This research line opens the path to exploring the correlations between charge transport and nonequilibrium, possibly quantum, regimes of the localized electromagnetic radiation. The corresponding hybrid devices are also promising for implementing quantum transducers, in which single-electrons control photonic quantum states.

II. THE SYSTEM

In this context, we analyze a parallel double quantum dot system, as shown in Fig. 1(a), in which each dot is capacitively coupled to one of two separated microwave cavities of resonance frequencies ω_a and ω_b , respectively. The two dots are connected to a common left and right lead with the hopping parameter t . We denote the cou-

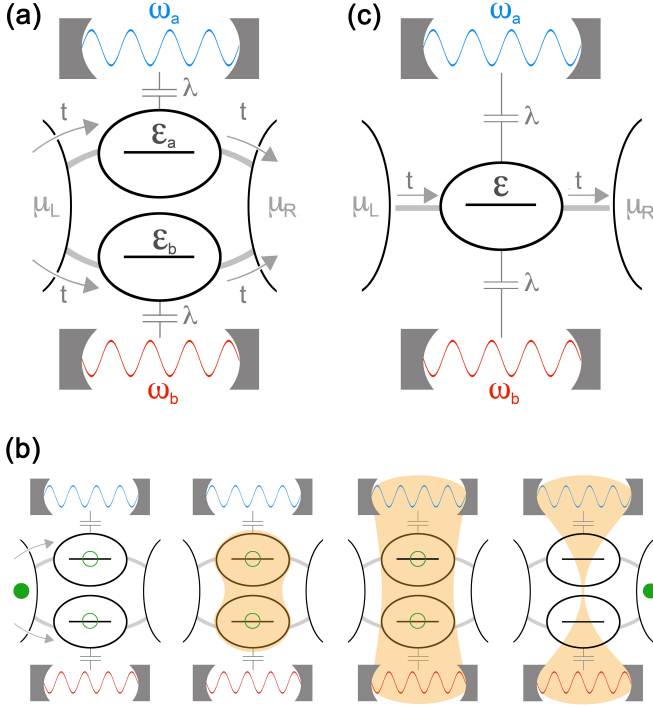


FIG. 1. Sketch of studied systems and idea. (a) Main model: a parallel double quantum dot with a single electronic energy level in each quantum dot. Each dot is coupled to one of two separated microwave cavities and a common left and right lead. (b) Basic idea: An electron travels through both branches of the parallel double quantum dot simultaneously. Its state is a coherent superposition of the states in the two dots. The delocalization of the single electron yields quantum correlations between the two cavities and remains even when the electron leaves the system. (c) Single quantum dot with a single electronic energy level coupled to two microwave cavities.

pling strength of the dot-cavity interaction by λ .

The local Coulomb repulsion in each dot shall be so large that double occupation is excluded. We therefore assume a single electron state (spinless) in each dot, whose energy level is given by $\epsilon_{a,b} = \bar{\epsilon} \pm \Delta\epsilon$ for the upper and lower dot, respectively. There is no direct tunneling between the dots and no interdot Coulomb interaction. This means that, a priori, we cannot exclude the possibility that both dots are occupied simultaneously. However, the tunnelling of two electrons into the two separate dots is an uncorrelated event and therefore cannot generate quantum correlations between the two microwave cavities.

We explore how correlation and entanglement between the two cavities emerge by the coherent transport of a single electron passing simultaneously through the two different dots. Let us first assume that the energy levels of the dots are close to each other, in the sense that the energy difference is small compared to their broadening $|\epsilon_a - \epsilon_b| \ll \Gamma$, i.e. the energy distributions overlap. In this regime the two paths are indistinguishable, and the elec-

tron flows through both branches simultaneously, causing quantum interference in the double quantum dot system. This means that, for example, the linear conductance associated with the two levels of the double dot system is different from the sum of the two linear conductances of the two separate dots (in the single level regime). If the difference between the two energy levels is increased, i.e. $|\epsilon_a - \epsilon_b| \gg \Gamma$, the interference is destroyed, and the electron transfer occurs via the incoherent (statistical) sum of the two possible paths, namely through the upper or through the lower branch, but not simultaneously through both. As we will see later, this is the mechanism that allows or prevents entanglement.

As illustrated in Fig. 1(b), the idealized procedure is as follows: When the electron travels inside the system, it splits. Therefore the electronic state is a coherent superposition of the electron occupying the upper dot or the lower dot, with the corresponding occupations $n_a^{(el)}$ and $n_b^{(el)}$. The state of the complete system is this superposed electron state coupled to the two ground states of the cavities $|\text{GS}\rangle_a$ and $|\text{GS}\rangle_b$.

$$|\Psi\rangle_{\text{in}} = \frac{1}{\sqrt{2}} \left(\left| n_a^{(el)} = 1, n_b^{(el)} = 0 \right\rangle + \left| n_a^{(el)} = 0, n_b^{(el)} = 1 \right\rangle \right) |\text{GS}\rangle_a |\text{GS}\rangle_b. \quad (1)$$

The interaction between an electron in a dot and the corresponding cavity ensures that a coherent state is created, depending on the position of the electron, described by the unitary evolution operator

$$U(\tau) = D_a[\hat{n}_a^{(el)}\rho(\tau)] \times D_b[\hat{n}_b^{(el)}\rho(\tau)], \quad (2)$$

where $\hat{n}_a^{(el)}$ and $\hat{n}_b^{(el)}$ are the electron occupation operators of the two dots, $D_{a,b}[\xi]$ are the coherent displacement operators with the associated parameter ξ , and $\rho(t) = -i\lambda t$. (Note that we set $\hbar = 1$ here and in the following.) After some dwell time τ the state has evolved, and the dot-cavity interaction correlates the two cavities,

$$U(\tau) |\Psi\rangle_{\text{in}} = \frac{1}{\sqrt{2}} \left(\left| n_a^{(el)} = 1, n_b^{(el)} = 0 \right\rangle |\rho(\tau)\rangle_a |\text{GS}\rangle_b + \left| n_a^{(el)} = 0, n_b^{(el)} = 1 \right\rangle |\text{GS}\rangle_a |\rho(\tau)\rangle_b \right), \quad (3)$$

where $|\rho(\tau)\rangle_a$ and $|\rho(\tau)\rangle_b$ are coherent states of the cavities. The quantum delocalization of the single electron in the double dot leads to a quantum correlation of the two cavities, which indicates the possibility of an entangled state. This state can persist even when the electron leaves the system and the dot state is empty,

$$|\Psi\rangle_{\text{out}} = \frac{1}{\sqrt{2}} |0, 0\rangle (|\rho(\tau)\rangle_a |\text{GS}\rangle_b + |\text{GS}\rangle_a |\rho(\tau)\rangle_b). \quad (4)$$

When a second electron enters the double dot, one can repeat a similar argument starting from the entangled

photon state instead of the vacuum. However, for long times, the internal losses of the cavities should be included as well as their energy relaxation and dephasing due to the coupling with the conducting leads via the double dot. In other words, Fig. 1(b) describes just the idealized argument of the entanglement generation process, where it is assumed that the interaction time of the electron and the cavity is short and that decoherence effects of the dots happen much later regarding the timescale of the interaction.

To investigate the possibility of entanglement, we will evaluate two quantities: We prove correlation via the covariance of the Fock occupation numbers and quantum correlation via the violation of the classical Cauchy-Schwarz inequality [37] for the two cavities. We calculate these two quantities by a perturbative expansion in the Keldysh Green's function formalism. To understand the underlying mechanism of the entanglement generation, we compare the results of the double quantum dot system for degenerated levels, namely zero energy difference of the two levels, with those of a large energy level difference. In addition, we discuss the results for a single quantum dot coupled to two cavities, see Fig. 1(c).

III. THEORETICAL MODEL

A. Basic Formalism

The double quantum dot system is described by a modified Anderson-Holstein Hamiltonian including the electronic and cavity part as well as the electron-photon interaction

$$\hat{H} = \hat{H}_{\text{el}} + \hat{H}_{\text{cav}} + \hat{H}_{\text{int}}, \quad (5)$$

$$\begin{aligned} \hat{H}_{\text{el}} = & \sum_{r=L,R} \sum_k (\varepsilon_{kr} - \mu_r) \hat{c}_{kr}^\dagger \hat{c}_{kr} + \sum_{\alpha=a,b} \varepsilon_\alpha \hat{d}_\alpha^\dagger \hat{d}_\alpha \\ & + t \sum_{r=L,R} \sum_{\alpha=a,b} \sum_k \left(\hat{c}_{kr}^\dagger \hat{d}_\alpha + \text{h.c.} \right), \end{aligned} \quad (6)$$

$$\hat{H}_{\text{cav}} = \sum_{\alpha=a,b} \omega_\alpha \hat{\alpha}^\dagger \hat{\alpha}, \quad (7)$$

$$\hat{H}_{\text{int}} = \lambda \sum_{\alpha=a,b} (\hat{\alpha}^\dagger + \hat{\alpha}) \hat{d}_\alpha^\dagger \hat{d}_\alpha. \quad (8)$$

Here, \hat{c}_{kr}^\dagger and \hat{d}_α^\dagger with $r = L, R$ and $\alpha = a, b$, are the creation operators of the electrons in the left and right lead and in the two quantum dots with energy levels ε_α . $\hat{\alpha}^\dagger$ and $\hat{\alpha}$ are the creation and annihilation operators of photons with frequency ω_α in cavity α . $t \in \mathbb{R}$ is the hopping parameter describing the transport of an electron between dots and leads. The voltage that is applied along the system shifts the electrochemical potential of the leads. We consider a symmetric shift in the high voltage limit

$$\mu_L = -\mu_R = \lim_{eV \rightarrow \infty} eV/2. \quad (9)$$

Therefore the Fermi functions of the left and right lead become $f_L(E) = 1$ and $f_R(E) = 0$. This approximation holds as long as the potential is the largest energy scale involved in our model, namely $|eV| \gg \max(k_B T, \Gamma, \Delta\varepsilon, \hbar\omega_0, \eta)$. Here $k_B T$ is the temperature of the leads, and η is the damping parameter that characterizes the cavity losses (see below). The origin of the dot energy levels is chosen to be in the middle of the electrochemical potentials of the two leads, i.e. $\bar{\varepsilon} = 0$. Dot energies are therefore specified only by the level difference, i.e. $\varepsilon_{a,b} = \pm\Delta\varepsilon$.

To determine the electronic transport through the system in the absence of electron-photon interaction, we calculate the unperturbed electronic Green's functions associated with the electronic part \hat{H}_{el} of the Hamiltonian, using the diagrammatic Keldysh technique and applying the wideband approximation for the leads [38, 39]. In this way we obtain the broadening Γ of the electronic levels. These electronic Green's functions represent our bare propagators in the perturbative approach, where we expand in terms of the electron-photon interaction. These unperturbed fermionic Green's functions $G_{\alpha\beta}(t_i, t_j) = -i\langle T_c(\hat{d}_\alpha(t)\hat{d}_\beta^\dagger(t')) \rangle$, beyond being in the matrix form of the Keldysh formalism [40], are also 2×2 matrices regarding the two parallel dots $\alpha, \beta = a, b$ [39]. T_c is the time-ordering operator with respect to the Keldysh contour. In a similar way, we define the single-particle bosonic Green's function $D_\alpha = -i\langle T_c(\hat{\alpha}(t)\hat{\alpha}^\dagger(t')) \rangle$ for the two cavities and the two-particle function $F_{\alpha\beta}(t, t') = -i\langle T_c(\hat{\alpha}(t)\hat{\beta}(t)\hat{\alpha}^\dagger(t')\hat{\beta}^\dagger(t')) \rangle$. We consider the two cavities with their intrinsic photon losses (damping), which leads to a finite broadening η of the unperturbed bosonic propagators. The explicit form of the unperturbed fermionic and bosonic Green's functions is given in Appendix A.

To demonstrate the entanglement of photons in the two cavities, we calculate the covariance

$$C = \langle \hat{n}_a \hat{n}_b \rangle - \langle \hat{n}_a \rangle \langle \hat{n}_b \rangle, \quad (10)$$

which proves correlation if it is finite, i.e. $C \neq 0$, and test the classical Cauchy-Schwarz inequality

$$S = \frac{\langle \hat{a}^\dagger \hat{a} \hat{b}^\dagger \hat{b} \rangle}{\sqrt{\langle \hat{a}^\dagger \hat{a} \hat{a}^\dagger \hat{a} \rangle} \sqrt{\langle \hat{b}^\dagger \hat{b} \hat{b}^\dagger \hat{b} \rangle}} \leq 1, \quad (11)$$

which proves quantum correlation if it is violated. In the expressions, the cavity occupations are defined by the bosonic operators $\hat{n}_a = \hat{a}^\dagger \hat{a}$ and $\hat{n}_b = \hat{b}^\dagger \hat{b}$, and S is the Cauchy-Schwarz parameter.

To calculate the expressions in Eqs. (10) and (11), we express the expectation values by Keldysh Green's functions and perform a diagrammatic perturbative expansion in the dot-cavity coupling λ up to fourth order. The expectation values in these equations are related to the lesser Green's functions in the limit of equal times of the single-particle and two particle Green's functions [40]. In this representation, the average photon number of a

single cavity $\langle \hat{n}_\alpha \rangle$, the covariance C and the Cauchy-Schwarz parameter S read

$$\langle \hat{n}_\alpha \rangle = D_\alpha^<(t, t), \quad (12)$$

$$C = (iF_{ab}^<(t, t) + D_a^<(t, t)D_b^<(t, t)), \quad (13)$$

$$S = \frac{F_{ab}^<(t, t)}{\sqrt{(F_{aa}^<(t, t)F_{bb}^<(t, t))}}. \quad (14)$$

The conditions for entanglement are a nonzero covariance, $C \neq 0$, and a violated classical Cauchy-Schwarz inequality, i.e. $S > 1$. The covariance and Cauchy-Schwarz parameter have no finite contributions in first or second order, so we have to calculate these quantities consistently up to the fourth order in λ .

B. Perturbation Expansion

For the single-particle bosonic Green's functions in Eqs. (12) and (13) we perform a perturbation expansion up to second order and for the two-particle Green's function in Eqs. (13) and (14) up to fourth order with respect to the dot-cavity interaction Hamiltonian in the interaction picture

$$H_{\text{int}}(\tau) = \lambda \left[(\hat{a}^\dagger + \hat{a})\hat{d}_a^\dagger \hat{d}_a + (\hat{b}^\dagger + \hat{b})\hat{d}_b^\dagger \hat{d}_b \right]_\tau. \quad (15)$$

To calculate the expectation values of the long chains of field operator occurring in the perturbative expansion, we use Wick's theorem, which allows to decompose a contour-ordered string of creation and annihilation operators, derived from a quadratic Hamiltonian, into a sum over all possible pairwise products.

Every product corresponds to unperturbed fermionic Green's functions $G_{\alpha\beta}(t_i, t_j)$ and the bosonic Green's functions $D_\alpha(t_i, t_j)$ with t_i, t_j laying on the Keldysh contour. An expansion up to fourth order yields contributions with four bosonic and four fermionic Green's functions, integrated over four different time arguments distributed on the Keldysh contour. Exemplary we consider the integral

$$I(t, t') = \lambda^4 \oint_c \oint_c \oint_c \oint_c dt_1 dt_2 dt_3 dt_4 \\ D_a(t, t_1) D_b(t_2, t') D_b(t, t_3) D_a(t_4, t') \\ G_{ab}(t_4, t_3) G_{ba}(t_3, t_4) G_{ab}(t_1, t_2) G_{ba}(t_2, t_1), \quad (16)$$

which contributes to the covariance and the classical Cauchy-Schwarz parameter, see the third diagram of Fig. 2. Parameterizing the contour, we transform the integrals from contour times to real times. The real-time integrals can be represented as Feynman diagrams. We get three different geometries, depicted in Fig. 2.

Due to the fourth order of the perturbative expansion we get four interaction points proportional to λ . This shows that we are dealing with a two-photon process,

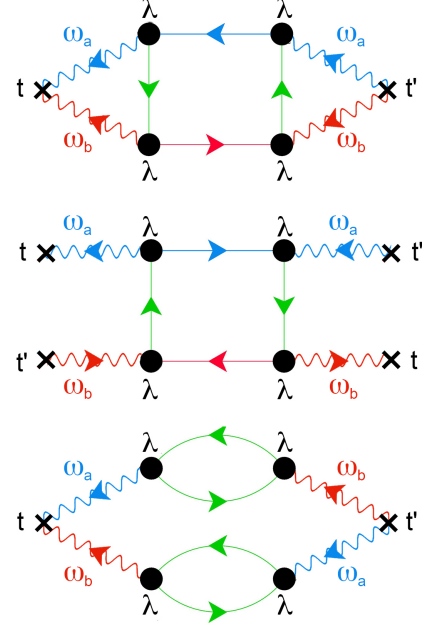


FIG. 2. Examples of vertex diagrams, which correspond to the integrals of the covariance and of the Cauchy-Schwarz parameter. The black dots represent the electron-photon interaction at time arguments laying on the Keldysh contour, which is proportional to λ . The wiggled lines correspond to the bosonic Green's functions of the microwave cavities with resonance frequency $\omega_{a,b}$, distinguished by the colors red and blue. The straight lines correspond to the fermionic Green's functions of the double quantum dot system, where we have four different components. Diagonal ones are indicated by blue and red lines, offdiagonal Green's functions are represented in green.

emitting and absorbing photons in both cavities a and b with corresponding energies $\omega_{a,b}$, which we distinguish by the red and blue wiggled lines. The process is described by different types of fermionic interaction in the double quantum dot system, represented by straight lines. Red and blue colors belong to the diagonal and the green lines to the off-diagonal elements of the Green's functions.

Several different vertex diagrams contribute to the covariance and the classical Cauchy-Schwarz parameter. The complete formulas for these two quantities in terms of unperturbed Green's functions are reported in Appendix B.

IV. RESULTS

To certain limits, we are able to calculate the relevant quantities analytically. We consider equal resonance frequencies $\omega_a = \omega_b \equiv \omega_0$ and zero temperature of the cavities. Furthermore we focus on the regime of low damping, i.e. $\omega_0 \gg \Gamma \gg \eta$, where η is the damping of the cavities, and the high voltage bias limit. Regarding the energy levels of the parallel quantum dots we consider two dif-

	DQD, $\Delta\varepsilon = 0$	DQD, $\Delta\varepsilon \gg \Gamma$	single dot
\bar{n}	n_0	$\bar{n}_s = 2n_0$	
δn^2	$n_0(1 - n_0/4)$	$\bar{n}_s(1 + \bar{n}_s/2)$	$\bar{n}_s(1 + 2\bar{n}_s)$
F	$1 - n_0/4$	$1 + \bar{n}_s/2$	$1 + 2\bar{n}_s$
C	$n_0/2$	0	$2\bar{n}_s^2$
S	2	2/3	1

TABLE I. Results for the average photon number of a single cavity \bar{n} , the fluctuations δn^2 , the Fano factor F , the covariance C and the Cauchy-Schwarz parameter S , for three different cases: the double quantum dot (DQD) coupled to two cavities with zero or large level spacing and a single quantum dot coupled to two cavities. See Fig. 1 for sketches of the systems. The parameter $n_0 = \pi^2 \left(\frac{\lambda}{\omega_0}\right)^2 \left(\frac{\Gamma}{\eta}\right)$.

ferent cases: First we study the case of two almost equal energy levels and second the case for two strongly differing levels. Finally, we compare these results with the case of a single dot coupled to two cavities at the same time.

We first determine the average photon number of the single cavities $\langle \hat{n}_a \rangle = \langle \hat{n}_b \rangle = \bar{n}$ up to second order and the corresponding fluctuations $\delta n^2 = \langle \hat{n}^2 \rangle - \bar{n}^2$ up to fourth order. The latter quantity can be easily computed from the knowledge of \bar{n} and $\langle \hat{\alpha}^\dagger \hat{\alpha}^\dagger \hat{\alpha} \hat{\alpha} \rangle$ (viz. $F_{\alpha\alpha}^<(t, t)$). Then one can analyze the behavior of the Fano factor, defined as $F = \delta n^2 / \bar{n}$. Finally, we calculate the covariance C and the Cauchy-Schwarz parameter S both up to fourth order in λ . Due to the symmetries in the system, the results for both cavities are the same.

In the first three lines of table I we show the results for the average occupation of the single cavities \bar{n} , their fluctuation, and the Fano factor. Let us discuss them successively in the following.

The average occupation for the single dot and the double dot with large level spacing are equal, since we calculate the average occupation only up to second order. The result of the double dot with two almost equal energy levels, i.e. $\Delta\varepsilon \ll \Gamma$, acting as single-electron splitter, is half the size of the case $\Delta\varepsilon \gg \Gamma$ and the single-dot system, i.e. $\bar{n}_0 = \bar{n}_s/2$. This becomes clear when we consider the electronic Hamiltonian of the parallel double dot coupled to the two leads. In the case of zero or small level spacing the Hamiltonian can be written in the form of an effective single-dot problem. Compared to the real single-dot case the dot-lead coupling parameter t is renormalized, i.e. $t_d = t_s/\sqrt{2}$. With $\Gamma \propto |t|^2$ this renormalization enters as a factor of two in the bosonic occupation of the cavi-

ties [39]. Furthermore we checked that the result for \bar{n}_s coincides with previous results in the limit, in which the induced damping (losses) associated with the electron-boson interaction is smaller than the intrinsic damping of the cavities η [41, 42].

According to table I, for the fluctuations and the corresponding Fano factor of the double-dot system we find a sub-Poissonian behavior in the regime, where we have quantum coherent transport through the double dot (interferometer regime) whereas we obtain a super-Poissonian behavior for the other two cases. The sub-Poissonian behavior corresponds to a photon antibunching in the local cavity. Let us emphasize that the nature of the interaction already appears at the level of a single-cavity quantity, namely the local fluctuations of the photons in a cavity. This fact can already be seen at two trivial examples, since the sub-Poissonian behavior occurs both for the entangled bosonic states in the Fock occupation $|\Psi\rangle_{pq} \sim |n_a = p, n_b = q\rangle + |n_a = q, n_b = p\rangle$ with $p, q \in \mathbb{N}$ or in the coherent state basis $|\Psi\rangle_{z_1 z_2} \sim |\xi_a = z_1, \xi_b = z_2\rangle + |\xi_a = z_2, \xi_b = z_1\rangle$, with $|\xi\rangle$ being a coherent state and $z_1, z_2 \in \mathbb{C}$.

For the covariance C we found a finite and positive value for the double quantum dot with two equal energy levels, which verifies a correlation of the photons in the single cavities. The covariance for a large level spacing vanishes, meaning that there is no correlation. This result is expected for the case of two separated electron pathways. Notice however that a finite covariance also arises in the case of a single dot simultaneously coupled to two cavities, see Fig. 1(c). This latter result can be interpreted as classical correlation, as we have a single photon emitter coupled to both cavities.

The ratio of the dot-cavity coupling constant λ and the resonance frequency ω_0 contributes with a power of 4 to the covariance of the parallel double quantum dot. This is based on the fourth order of the perturbative expansion, and we could have expected this dependence from the Feynman diagrams, see Fig. 2. The broadening of the electronic level Γ , divided by the damping of the oscillators η , is both for the double-dot and single-dot cases proportional to the power of 2, since the double-dot system for equal energy levels effectively behaves like a single-dot problem, both with two couplings t to the two leads.

A finite covariance proves correlation but does not indicate quantum correlation (entanglement). To distinguish classical and quantum correlations, we calculated the classical Cauchy-Schwarz parameter S of Eq. (14), which we cast in the following form

$$S = \frac{|\bar{n}^2 + C|}{|\bar{n}(\bar{n} - 1) + \delta n^2|} = \frac{|\bar{n} + \frac{C}{\bar{n}}|}{|\bar{n} + F - 1|}. \quad (17)$$

The expression states that a violated Cauchy-Schwarz inequality ($S > 1$) occurs, if a finite and positive covariance is combined with a sub-Poissonian ($F < 1$) behaviour. As reported in the first column of the last line of table I, the Cauchy-Schwarz inequality for vanishing level spacing in

the double dot system is clearly violated. This confirms the entanglement of the photons in the two distant microwave cavities, if the energy levels of the two dots are sufficiently close to each other, viz. the electron is delocalized over the two dots, when it flows from one lead to the other. For strongly differing energy levels of the dots, the classical Cauchy-Schwarz inequality is not longer violated as $C = 0$ (uncorrelated systems). As a sanity check, for the single dot with $C > 0$ and $F > 1$ (super-Poissonian) we find that the classical Cauchy-Schwarz inequality is not violated but reaches the maximum classical value.

V. SUMMARY

We studied single-electron transport through a parallel double quantum dot, each dot being coupled to a separate microwave cavity. We showed in a simple scheme that for degenerate dot energies, when quantum interference between the two transport pathways is most pronounced, the delocalized electron entangles the two separated microwave cavities. Using the Keldysh Green's function method and a perturbative expansion up to fourth order in the dot-cavity interaction strength, we demonstrated quantum correlations between the cavities through a nonzero covariance and the violation of the classical Cauchy-Schwarz inequality. Due to the complexity of the calculations we presented results only for the perfectly symmetric case, with both quantum dots exhibiting equal energy levels. But we expect that our findings are still valid, if the degeneracy is lifted and the system becomes slightly asymmetric. For too large level detunings or a single dot coupled to two cavities, we have shown that the photons in the different cavities cannot be entangled.

ACKNOWLEDGMENTS

The work was supported by the Deutsche Forschungsgemeinschaft (DFG, German Research Foundation) through Project-ID 32152442 - SFB 767 and Project-ID 25217212 - SFB 1432, and by the German Excellence Strategy via the Zukunftskolleg of the University of Konstanz.

Appendix A: Green's Functions

1. Fermionic subsystem

We determine the bare fermionic Green's functions of the double quantum dot system and the bare bosonic Green's functions of the single cavities separately, using the diagrammatic Keldysh Green's function technique. The fermionic Keldysh Green's function is a 2×2 matrix in Keldysh space

$$\check{G}(E) = \begin{pmatrix} G(E) & G^<(E) \\ G^>(E) & \tilde{G}(E) \end{pmatrix}, \quad (\text{A1})$$

representing the Fourier transformations of the time-ordered $G(t, t')$, anti-time-ordered $\tilde{G}(t, t')$, lesser $G^<(t, t')$ and greater $G^>(t, t')$ Greens functions. Each component in turn is again a 2×2 matrix in the subspace of the parallel double quantum dot, i.e. for the time-ordered Green's function

$$G(E) = \begin{pmatrix} G_{aa}(E) & G_{ab}(E) \\ G_{ba}(E) & G_{bb}(E) \end{pmatrix}, \quad (\text{A2})$$

where $\alpha, \beta = a, b$ in $G_{\alpha\beta}(E)$ refer to the upper or lower dot, respectively, see Fig. 1(a).

We consider the Keldysh Green's function in the high voltage bias limit. For this reason the Fermi functions of the left and right lead become $f_L(E) = 1$ and $f_R(E) = 0$. $\Gamma \propto |t|^2$ is the broadening of the electronic levels from the coupling to the electrodes, which is treated symmetrically for both sides. Under these conditions the greater and lesser Green's functions read

$$G^<(E) = -G^>(E) = \frac{i\Gamma}{(E^2 - \Delta\varepsilon^2)^2 + 4\Gamma^2 E^2} \quad (\text{A3})$$

$$\cdot \begin{pmatrix} (E + \Delta\varepsilon)^2 & (E^2 - \Delta\varepsilon^2) \\ (E^2 - \Delta\varepsilon^2) & (E - \Delta\varepsilon)^2 \end{pmatrix}, \quad (\text{A4})$$

and the time-ordered and anti-time-ordered Green's functions

$$G(E) = -\tilde{G}(E) = \frac{1}{(E^2 - \Delta\varepsilon^2)^2 + 4\Gamma^2 E^2} \quad (\text{A5})$$

$$\cdot \begin{pmatrix} (E - \Delta\varepsilon)(E + \Delta\varepsilon)^2 + 2\Gamma^2 E & -2\Gamma^2 E \\ -2\Gamma^2 E & (E - \Delta\varepsilon)^2(E + \Delta\varepsilon) + 2\Gamma^2 E \end{pmatrix}. \quad (\text{A6})$$

2. Bosonic Green's functions

We define the time dependent bosonic Keldysh Green's functions as

$$\check{D}(t, t') = \begin{pmatrix} D(t, t') & D^<(t, t') \\ D^>(t, t') & \tilde{D}(t, t') \end{pmatrix} \quad (\text{A7})$$

$$= -i \begin{pmatrix} \langle T_c(\alpha^\dagger(t')\alpha(t)) \rangle & \langle \alpha^\dagger(t')\alpha(t) \rangle \\ \langle \alpha(t)\alpha^\dagger(t') \rangle & \langle \tilde{T}_c(\alpha^\dagger(t')\alpha(t)) \rangle \end{pmatrix}, \quad (\text{A8})$$

with T_c and \tilde{T}_c being the time-ordering and anti-time-ordering operator. For a time independent Hamiltonian, as considered here, $\check{D}(t, t')$ and all of its components will just depend on the time difference $t - t'$. To obtain the bosonic Green's functions in energy space, we calculate the Fourier transformation with respect to the time difference, yielding

$$D_\alpha^<(E) = \frac{-in_\alpha\eta}{(E - \omega_\alpha) + \eta^2}, \quad (\text{A9})$$

$$D_\alpha^>(E) = \frac{-i(n_\alpha + 1)\eta}{(E - \omega_\alpha) + \eta^2}, \quad (\text{A10})$$

$$D_\alpha(E) = \frac{E - \omega_\alpha - i\eta(2n_\alpha + 1)}{(E - \omega_\alpha)^2 + \eta^2}, \quad (\text{A11})$$

$$\tilde{D}_\alpha(E) = \frac{-(E - \omega_\alpha) - i\eta(2n_\alpha + 1)}{(E - \omega_\alpha)^2 + \eta^2}. \quad (\text{A12})$$

If the cavity is coupled to an external bath, as for instance a transmission line into which photons from the cavity escape, the bosonic Green's functions contain an imaginary part $\pm i\eta$, as used in the expressions above, which describes the damping of the cavity resonator.

We treat the cavities at zero temperature, such that the initial photon number n_α is zero. Since we are interested only in the lesser functions, compare Eqs. (12) to (14) and $n_\alpha = 0$, in the final formulas of the integrals only the time-ordered and anti-time-ordered bosonic Green's functions

$$D_\alpha(E) = \frac{1}{E - \omega_\alpha + i\eta}, \quad \tilde{D}_\alpha(E) = -\frac{1}{E - \omega_\alpha - i\eta} \quad (\text{A13})$$

will contribute.

Appendix B: Perturbation Expansion

For each Green's function in Eqs. (12) to (14) we perform a perturbative expansion with respect to the dot-cavity interaction Hamiltonian in Eq. (15). Since the

second order contributions of C and S are zero, we calculate up to fourth order. Regarding Eq. (15) we get integrals over a long chain of bosonic and fermionic creation and annihilation operators. We can transform the expectation values into a sum over products of four time-dependent fermionic and four bosonic Green's functions using Wick's theorem. The integrals can be represented as Feynman diagrams. Exemplary, we display the diagrams that determine the covariance in Fig. (3). To distinguish the different types of Green's functions occurring, we use straight lines for the fermionic and wiggled lines for the bosonic. Since we have two cavities and the fermionic Green's functions have four components, describing the parallel double quantum dot subspace, we introduce the following color code: (i) Light blue color for the bosonic Green's function of the upper cavity ($\check{D}_a(E)$) and the diagonal element of the fermionic Green's function of the upper quantum dot ($\check{G}_{aa}(E)$). (ii) Red color for the bosonic Green's function of the lower cavity ($\check{D}_b(E)$) and the diagonal element of the fermionic Green's function for the lower quantum dot ($\check{G}_{bb}(E)$). (iii) Light green color for the two off-diagonal elements of the fermionic Green's function ($\check{G}_{ab}(E)$, $\check{G}_{ba}(E)$).

The integrals that contribute to the covariance are visualized in terms of vertex diagrams in Fig. 3. The structure of the diagrams for the Cauchy-Schwarz parameter S is similar, but they differ in the composition of the components of the Green's functions. Due to the fourth order of the perturbative expansion we get four interaction points proportional to the dot-cavity coupling strength λ . The diagrams thus describe a two-photon process, involving the emission and absorption of photons in both cavities with energy ω_0 , and different types of fermionic interaction in the double quantum dot system. Parametrizing the Keldysh contour through

$$\int_c d\tau = \int_{-\infty}^{\infty} dt^+ + \int_{\infty}^{-\infty} dt^-, \quad (\text{B1})$$

where t^+ are time arguments on the upper branch and t^- on the lower branch of the contour, we transform the integrals from contour time to real time and subsequently sum up the integrand for all possible configurations of the integration variables t_1 to t_4 on the contour. Regarding Eqs. (12) to (14), two time arguments are already fixed due to the choice of the lesser component. This and the fact that the bosonic lesser Green's function of Eq. (A9) is zero reduces the number of possible configurations of time arguments on the contour to only one. With the Fourier transformation we express the integrals in energy space.

The average occupation of each cavity is calculated up to second order, where \bar{n}_a corresponds to the upper (blue) branch of the first diagram in Fig. 3 and \bar{n}_b to the lower (red) branch. We consider the limit of equal resonance frequencies $\omega_a = \omega_b \equiv \omega_0$. Therefore the expressions for the bosonic Green's functions of Eqs. (A9) to (A12) become independent of α , i.e. equal for both cavities. The average occupations for the two cavities $\alpha = a, b$ read up

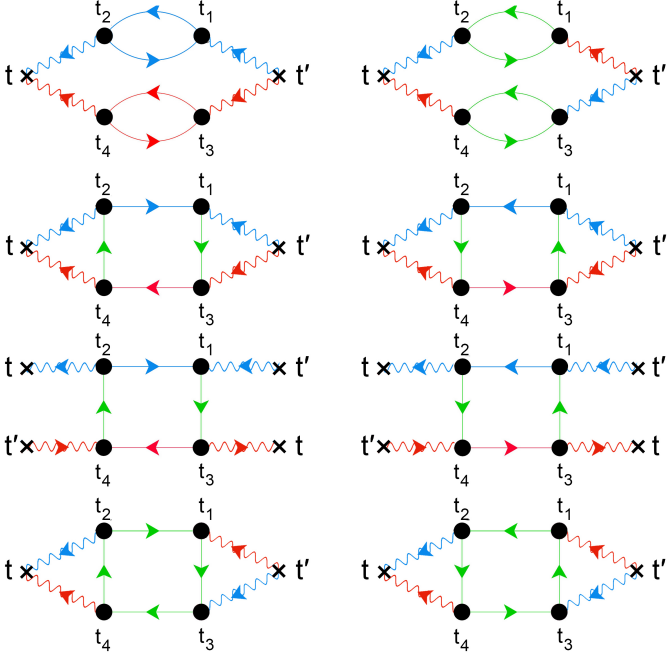


FIG. 3. Eight different vertex diagrams representing the eight integrals that determine the covariance C . The black dots represent the electron-photon interaction at a time arguments t_1 to t_4 laying on the upper (+) or lower (-) branch of the Keldysh contour and is proportional to λ . The wiggled lines correspond to the bosonic Green's functions of the microwave cavities with resonance frequency $\omega_{a,b}$, and the straight lines to the fermionic Green's functions of the double quantum dot system.

to second order

$$\bar{n}_\alpha = -\lambda^2 \iint d\omega_1 d\omega_2 D(\omega_2 - \omega_1) G_{\alpha\alpha}^<(\omega_2) G_{\alpha\alpha}^<(\omega_1) \tilde{D}(\omega_2 - \omega_1). \quad (\text{B2})$$

They become identical for zero level spacing $\bar{n}_a = \bar{n}_b$, since also the Green's functions of the two dots, the diagonal elements of Eq. (A4), are equivalent. For a large level spacing the quantities have to be calculated separately.

To determine the covariance, we need in addition the perturbative expression of $\langle \hat{n}_a \hat{n}_b \rangle$ up to fourth order. It is given by

$$\begin{aligned} \langle \hat{a}^\dagger \hat{a} \hat{b}^\dagger \hat{b} \rangle &= \lambda^4 \iiint d\omega_1 d\omega_2 d\omega_3 d\omega_4 \{ \\ &D(\omega_1 - \omega_2) D(\omega_3 - \omega_4) \tilde{D}(\omega_1 - \omega_2) \tilde{D}(\omega_3 - \omega_4) [G_{aa}^<(\omega_1) G_{aa}^<(\omega_2) G_{bb}^<(\omega_3) G_{bb}^<(\omega_4) + G_{ab}^<(\omega_3) G_{ab}^<(\omega_2) G_{ab}^<(\omega_1) G_{ab}^<(\omega_4)] \\ &+ D(\omega_1 - \omega_2) D(\omega_3 - \omega_4) \tilde{D}(\omega_1 - \omega_4) \tilde{D}(\omega_3 - \omega_2) [G_{aa}^<(\omega_1) G_{ab}^<(\omega_2) G_{bb}^<(\omega_3) G_{ab}^<(\omega_4) + G_{ab}^<(\omega_3) G_{aa}^<(\omega_2) G_{ab}^<(\omega_1) G_{bb}^<(\omega_4)] \\ &+ D(\omega_1 - \omega_2) D(\omega_2 - \omega_4) \tilde{D}(\omega_1 - \omega_3) \tilde{D}(\omega_3 - \omega_4) \\ &G_{ab}(\omega_2) G_{ab}(\omega_3) [G_{aa}^<(\omega_1) G_{bb}^<(\omega_4) + G_{aa}^<(\omega_4) G_{bb}^<(\omega_1) + 2 G_{ab}^<(\omega_1) G_{ab}^<(\omega_4)] \}. \end{aligned} \quad (\text{B3})$$

The two bubble diagrams in the first line of Fig. 3, which correspond to the expressions in the first line of Eq. (B3), are factorizable and can be separated into

their upper and lower branches. This leads to two two-dimensional integrals, which are equal or similar to the integral of the average occupation of Eq. (B2).

To determine the Cauchy-Schwarz parameter, fluctuations and the Fano factor we need to evaluate furthermore

$$\begin{aligned} \langle \hat{\alpha}^\dagger \hat{\alpha}^\dagger \hat{\alpha} \hat{\alpha} \rangle &= 2\lambda^4 \iiint d\omega_1 d\omega_2 d\omega_3 d\omega_4 \left\{ \right. \\ &2D(\omega_1 - \omega_2)D(\omega_2 - \omega_3)\tilde{D}(\omega_4 - \omega_3)\tilde{D}(\omega_1 - \omega_4)G_{\alpha\alpha}(\omega_4)G_{\alpha\alpha}^<(\omega_1)G_{\alpha\alpha}(\omega_2)G_{\alpha\alpha}^<(\omega_3) \\ &+ [D(\omega_1 - \omega_2)D(\omega_3 - \omega_4)G_{\alpha\alpha}^<(\omega_1)G_{\alpha\alpha}^<(\omega_3)G_{\alpha\alpha}^<(\omega_2)G_{\alpha\alpha}^<(\omega_4)] [\tilde{D}(\omega_1 - \omega_2)\tilde{D}(\omega_3 - \omega_4) + \tilde{D}(\omega_1 - \omega_4)\tilde{D}(\omega_3 - \omega_2)] \left. \right\}, \end{aligned} \quad (\text{B4})$$

for $\alpha = \text{a,b}$. We evaluate the two-dimensional integral over energy required for the average occupation in Eq. (B2) and the separable terms of Eqs. (B3) and (B4) as well as the four-dimensional integrals of the eight Green's functions in Eqs. (B3) and (B4) using the Residue theo-

rem. The long and complex expressions occurring after the integrations are then simplified in the low damping limit $\omega_0 \gg \Gamma \gg \eta$, finally yielding the results quoted in table I.

-
- [1] A. W. Holleitner, C. R. Decker, H. Qin, K. Eberl, and R. H. Blick, Coherent Coupling of Two Quantum Dots Embedded in an Aharonov-Bohm Interferometer, *Phys. Rev. Lett.* **87**, 256802 (2001).
 - [2] M. Sigrist, T. Ihn, K. Ensslin, M. Reinwald, and W. Wegscheider, Coherent Probing of Excited Quantum Dot States in an Interferometer, *Phys. Rev. Lett.* **98**, 036805 (2007).
 - [3] T. Hatano, T. Kubo, Y. Tokura, S. Amaha, S. Teraoka, and S. Tarucha, Aharonov-Bohm Oscillations Changed by Indirect Interdot Tunneling via Electrodes in Parallel-Coupled Vertical Double Quantum Dots, *Phys. Rev. Lett.* **106**, 076801 (2011).
 - [4] Y. Ji, Y. Chung, D. Sprinzak, M. Heiblum, D. Mahalu, and H. Shtrikman, An electronic Mach-Zehnder interferometer, *Nature* **422**, 415 (2003).
 - [5] R. Schuster, E. Buks, M. Heiblum, D. Mahalu, V. Umansky, and H. Shtrikman, Phase measurement in a quantum dot via a double-slit interference experiment, *Nature* **385**, 417 (1997).
 - [6] E. Bocquillon, V. Freulon, J. M. Berroir, P. Degiovanni, B. Plaçais, A. Cavanna, Y. Jin, and G. Fève, Coherence and indistinguishability of single electrons emitted by independent sources, *Science* **339**, 1054 (2013).
 - [7] A. Blais, A. L. Grimsmo, S. M. Girvin, and A. Wallraff, Circuit quantum electrodynamics, *Rev. Mod. Phys.* **93**, 025005 (2021).
 - [8] M. Hofheinz, E. M. Weig, M. Ansmann, R. C. Bialczak, E. Lucero, M. Neeley, A. D. O'Connell, H. Wang, J. M. Martinis, and A. N. Cleland, Generation of Fock states in a superconducting quantum circuit, *Nature* **454**, 310 (2008).
 - [9] M. Hofheinz, H. Wang, M. Ansmann, R. C. Bialczak, E. Lucero, M. Neeley, A. D. O'Connell, D. Sank, J. Wenner, J. M. Martinis, and A. N. Cleland, Synthesizing arbitrary quantum states in a superconducting resonator, *Nature* **459**, 546 (2009).
 - [10] H. Wang, M. Mariani, R. C. Bialczak, M. Lenander, E. Lucero, M. Neeley, A. D. O'Connell, D. Sank, M. Weides, J. Wenner, T. Yamamoto, Y. Yin, J. Zhao, J. M. Martinis, and A. N. Cleland, Deterministic Entanglement of Photons in Two Superconducting Microwave Resonators, *Phys. Rev. Lett.* **106**, 060401 (2011).
 - [11] E. Zakka-Bajjani, F. Nguyen, M. Lee, L. R. Vale, R. W. Simmonds, and J. Aumentado, Quantum superposition of a single microwave photon in two different 'colour' states, *Nat. Phys.* **7**, 599 (2011).
 - [12] F. Nguyen, E. Zakka-Bajjani, R. W. Simmonds, and J. Aumentado, Quantum Interference between Two Single Photons of Different Microwave Frequencies, *Phys. Rev. Lett.* **108**, 163602 (2012).
 - [13] C. Eichler, D. Bozyigit, C. Lang, M. Baur, L. Steffen, J. M. Fink, S. Filipp, and A. Wallraff, Observation of Two-Mode Squeezing in the Microwave Frequency Domain, *Phys. Rev. Lett.* **107**, 113601 (2011).
 - [14] E. Flurin, N. Roch, F. Mallet, M. H. Devoret, and B. Huard, Generating Entangled Microwave Radiation Over Two Transmission Lines, *Phys. Rev. Lett.* **109**, 183901 (2012).
 - [15] C. Lang, C. Eichler, L. Steffen, J. M. Fink, M. J. Woolley, A. Blais, and A. Wallraff, Correlations, indistinguishability and entanglement in Hong-Oh-Mandel experiments at microwave frequencies, *Nat. Phys.* **9**, 345 (2013).
 - [16] C. Wang, Y. Y. Gao, P. Reinhold, R. W. Heeres, N. Ofek, K. Chou, C. Axline, M. Reagor, J. Blumoff, K. M. Sliwa, L. Frunzio, S. M. Girvin, L. Jiang, M. Mirrahimi, M. H. Devoret, and R. J. Schoelkopf, A Schrödinger cat living in two boxes, *Science* **352**, 1087 (2016).
 - [17] A. Peugeot, G. Ménard, S. Dambach, M. Westig, B. Kubala, Y. Mukharsky, C. Altimiras, P. Joyez, D. Vion, P. Roche, D. Esteve, P. Milman, J. Leppäkangas, G. Johansson, M. Hofheinz, J. Ankerhold, and F. Portier, Generating Two Continuous Entangled Microwave Beams Using a dc-Biased Josephson Junction, *Phys. Rev. X* **11**, 031008 (2021).
 - [18] J. R. Petta, A. C. Johnson, J. M. Taylor, E. A. Laird, A. Yacoby, M. D. Lukin, C. M. Marcus, M. P. Hanson, and A. C. Gossard, Coherent manipulation of coupled electron spins in semiconductor quantum dots, *Science* **309**, 2180 (2005).
 - [19] F. H. L. Koppens, C. Buizert, K. J. Tielrooij, I. T. Vink, K. C. Nowack, T. Meunier, L. P. Kouwenhoven, and L. M. K. Vandersypen, Driven coherent oscillations of a single electron spin in a quantum dot, *Nature* **442**, 766 (2006).

- (2006).
- [20] K. C. Nowack, F. H. L. Koppens, Y. V. Nazarov, and L. M. K. Vandersypen, Coherent control of a single electron spin with electric fields, *Science* **318**, 1430 (2007).
 - [21] G. Burkard, M. J. Gullans, X. Mi, and J. R. Petta, Superconductor–semiconductor hybrid-circuit quantum electrodynamics, *Nat. Rev. Phys.* **2**, 129 (2020).
 - [22] K. D. Petersson, L. W. McFaul, M. D. Schroer, M. Jung, J. M. Taylor, A. A. Houck, and J. R. Petta, Circuit quantum electrodynamics with a spin qubit, *Nature* **490**, 380 (2012).
 - [23] C. Rössler, D. Oehri, O. Zilberberg, G. Blatter, M. Karalic, J. Pijnenburg, A. Hofmann, T. Ihn, K. Ensslin, C. Reichl, and W. Wegscheider, Transport spectroscopy of a spin-coherent dot-cavity system, *Phys. Rev. Lett.* **115**, 166603 (2015).
 - [24] J. J. Viennot, M. C. Dartiailh, A. Cottet, and T. Kontos, Coherent coupling of a single spin to microwave cavity photons., *Science* **349**, 408 (2015).
 - [25] L. E. Bruhat, J. J. Viennot, M. C. Dartiailh, M. M. Desjardins, T. Kontos, and A. Cottet, Cavity Photons as a Probe for Charge Relaxation Resistance and Photon Emission in a Quantum Dot Coupled to Normal and Superconducting Continua, *Phys. Rev. X* **6**, 021014 (2016).
 - [26] D. Hagenmüller, S. Schütz, J. Schachenmayer, C. Genes, and G. Pupillo, Cavity-assisted mesoscopic transport of fermions: Coherent and dissipative dynamics, *Phys. Rev. B* **97**, 205303 (2018).
 - [27] M. Trif and P. Simon, Braiding of Majorana Fermions in a Cavity, *Phys. Rev. Lett.* **122**, 236803 (2019).
 - [28] W. Khan, P. Potts, S. Lehmann, K. Thelander, C. Dick, P. Samuelsson, and V. Maisi, Efficient and continuous microwave photoconversion in hybrid cavity-semiconductor nanowire double quantum dot diodes, *Nat. Commun.* **12**, 5130 (2021).
 - [29] A. Cottet, Z. Leghtas, and T. Kontos, Theory of interactions between cavity photons induced by a mesoscopic circuit, *Phys. Rev. B* **102**, 155105 (2020).
 - [30] O. Dmytruk, M. Trif, C. Mora, and P. Simon, Out-of-equilibrium quantum dot coupled to a microwave cavity, *Phys. Rev. B* **93**, 075425 (2016).
 - [31] J. Lu, R. Wang, J. Ren, M. Kulkarni, and J.-H. Jiang, Quantum-dot circuit-QED thermoelectric diodes and transistors, *Phys. Rev. B* **99**, 035129 (2019).
 - [32] B. Bhandari, P. A. Erdman, R. Fazio, E. Paladino, and F. Taddei, Thermal rectification through a nonlinear quantum resonator, *Phys. Rev. B* **103**, 155434 (2021).
 - [33] X. Mi, J. V. Cady, D. M. Zajac, P. W. Deelman, and J. R. Petta, Strong coupling of a single electron in silicon to a microwave photon, *Science* **355**, aal2469 (2016).
 - [34] A. Stockklauser, P. Scarlino, J. V. Koski, S. Gasparinetti, C. K. Andersen, C. Reichl, W. Wegscheider, T. Ihn, K. Ensslin, and A. Wallraff, Strong Coupling Cavity QED with Gate-Defined Double Quantum Dots Enabled by a High Impedance Resonator, *Phys. Rev. X* **7**, 011030 (2017).
 - [35] X. Mi, M. Benito, S. Putz, D. M. Zajac, J. M. Taylor, G. Burkard, and J. R. Petta, A coherent spin–photon interface in silicon, *Nature* **555**, 599 (2018).
 - [36] P. Scarlino, D. J. van Woerkom, A. Stockklauser, J. V. Koski, M. C. Collodo, S. Gasparinetti, C. Reichl, W. Wegscheider, T. Ihn, K. Ensslin, and A. Wallraff, All-Microwave Control and Dispersive Readout of Gate-Defined Quantum Dot Qubits in Circuit Quantum Electrodynamics, *Phys. Rev. Lett.* **122**, 206802 (2019).
 - [37] S. Wölk, M. Huber, and O. Gühne, Unified approach to entanglement criteria using the Cauchy-Schwarz and Hölder inequalities, *Phys. Rev. A* **90**, 022315 (2014).
 - [38] T. V. Shahbazyan and M. E. Raikh, Two-channel resonant tunneling, *Phys. Rev. B* **49**, 123 (1994).
 - [39] B. Kubala and J. König, Flux-dependent level attraction in double-dot Aharonov-Bohm interferometers, *Phys. Rev. B* **65**, 245301 (2002).
 - [40] J. Rammer, *Quantum Field Theory of Non-equilibrium States*, 1st ed. (Cambridge University Press, Cambridge, 2007).
 - [41] A. Mitra, I. Aleiner, and A. J. Millis, Phonon effects in molecular transistors: Quantal and classical treatment, *Phys. Rev. B* **69**, 245302 (2004).
 - [42] P. Stadler, W. Belzig, and G. Rastelli, Ground-State Cooling of a Carbon Nanomechanical Resonator by Spin-Polarized Current, *Phys. Rev. Lett.* **113**, 047201 (2014).